ACS APPLIED MATERIALS & INTERFACES

Research Article

www.acsami.org

Effect of Al_2O_3 Seed-Layer on the Dielectric and Electrical Properties of Ultrathin MgO Films Fabricated Using *In Situ* Atomic Layer Deposition

Jagaran Acharya,*[,†] Ryan Goul,[†] Devon Romine,[‡] Ridwan Sakidja,[‡] and Judy Wu*[,†]

[†]Department of Physics and Astronomy, University of Kansas, Lawrence, Kansas 66045, United States

[‡]Department of Physics, Astronomy and Materials Science, Missouri State University, Springfield, Missouri 65897, United States

Supporting Information

ABSTRACT: Metal/insulator/metal (M/I/M) trilayers of Al/MgO/Al with ultrathin MgO in the thickness range of 2.20−4.40 nm were fabricated using *in vacuo* sputtering and atomic layer deposition (ALD). In order to achieve a high-quality metal/insulator (M/I) interface and hence high-quality dielectric ALD-MgO films, a 5 cycles (∼0.55 nm) thick ALD-Al_2O_3 seed layer (SL) was employed to demonstrate the dielectric constant (ε_r) is ∼8.82−9.38 in 3.30−4.95 nm thick ALD-MgO/SL films, which is close to that of single-crystal MgO ε_r ∼ 9.80. In contrast, a low ε_r of 3.55−4.66 for the ALD-MgO films of a similar thickness without a SL was observed. The effective oxide thickness (EOT) of ∼1.40 nm has therefore been achieved in the ultrathin ALD-MgO films, which are comparable to the EOTs of high-K dielectrics such as HfO_2. In addition, the leakage current through the M/I/M structure is reduced by more than 1 order of magnitude with implementation of the SL. The high leakage current in the samples without a SL can be attributed to the nonuniform nucleation of the ALD-MgO on the Al surface with a significant portion of the Al surface remaining conductive as confirmed using *in vacuo* scanning tunneling spectroscopy (STS). With the SL, the STS study has confirmed a tunnel barrier height of 1.50 eV on 0.55 nm MgO with 0.55 nm Al_2O_3 SL with almost 100% coverage. In addition, molecular dynamics simulations point out the importance of deposition of ultrathin SL that has a significant effect on the initial nucleation of the Mg precursor. This result not only illustrates the critical importance of controlling the M/I interface to obtain high-quality dielectric properties of ultrathin ALD films but also provides an approach to engineering incompatible M/I interfaces using a SL for a high-quality dielectric required for applications in M/I/M tunnel junctions and complementary metal oxide semiconductors.

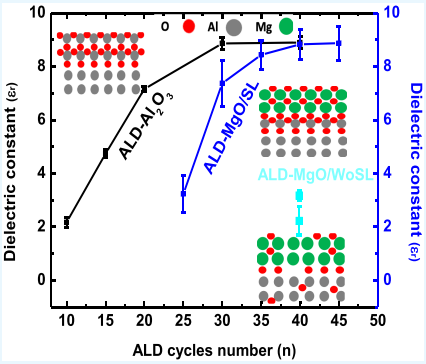

KEYWORDS: *in situ atomic layer deposition, ultrathin film, dielectric properties, metal/insulator interface, seed layer, capacitors, in vacuo*

INTRODUCTION

Following Moore's law, the further advancement of microelectronics toward reduced dimensions demands leak-free and defect-free ultrathin dielectric films with thickness in the range comparable or less than 5 nm dielectric films. Applications requiring such ultrathin dielectrics include metal/insulator/metal (M/I/M) tunnel junctions[1−6] and gate dielectrics in complementary metal-oxide-semiconductor (CMOS) technology.[7−9] Both physical vapor deposition such as magnetron sputtering,[10,11] molecular beam epitaxy,[2] and chemical vapor deposition (CVD) including atomic layer deposition (ALD)[1,3,4,6,11] are used for deposition of ultrathin dielectrics such as Al_2O_3, HfO_2, ZrO_2, MgO, etc. Among others, ALD is particularly suitable due to several unique advantages including low defect density through a well-controlled ligand-exchange mechanism on the sample surface with high conformality over surfaces with large aspect ratios and atomic-scale thickness control.[5−8,11−16] However, dielectric properties of ALD films are often considerably degraded with respect to their single-crystal bulk counterparts.[8,14−18] For example, in the M/I/M trilayers, the defective interfacial layer at the M/I interface, which may form during either *ex situ* growth of the "I" layers or *in vacuo* growth of the "M/I" bilayer under nonoptimal conditions, has been found to be detrimental to their dielectric properties.[12,13] Consequently, significantly lower dielectric constants (ε_r) than the single-crystal bulk values were reported on ALD dielectric ultrathin films.[8,14−18] Specifically, a monotonic decreasing of ε_r with decreasing the film thickness from tens of nanometers to the ultrathin regime has been observed.[17,18] These results indicate that the defective insulator layer (IL) must be eliminated in order to achieve high-quality films.

Magnesium oxide (MgO), with its wide band gap of 7.80 eV, ε_r of 9.80,[19,20] low refractive index, and high stability, is an

Received: April 2, 2019
Accepted: July 29, 2019
Published: July 29, 2019

ACS Publications © XXXX American Chemical Society

DOI: 10.1021/acsami.9b05601
ACS Appl. Mater. Interfaces XXXX, XXX, XXX−XXX

interesting dielectric for (M/I/M) tunnel junctions and other devices.[19−23] Specifically, MgO is the best tunnel barrier material for magnetic tunnel junctions (MTJs) to allow coherent tunneling of the spin current, which leads to significantly higher tunneling magnetoresistance up to 200%[2] in contrast to 70% in MTJs with Al_2O_3 as the tunnel barrier.[24] MgO has been deposited using CVD,[25] pulsed laser deposition,[26] homogeneous precipitation, sol−gel processes,[23] and ALD.[21,22] This has further motivated research in the growth of ultrathin ALD-MgO films. However, the investigation of the interface for ultrathin ALD-MgO films directly on the metal show formation of an interfacial layer with oxidation of the electrode.[27] A systematic study on the dielectric properties of ALD-MgO for MIM devices is lacking, which is possibly due to the difficulties to obtain leak-free ultrathin ALD-MgO films. However, the study of ALD-MgO in the thickness range of 4.6−11 nm on Si for metal oxide semiconductor capacitors shows an ε_r close to single-crystal bulk MgO.[27] Previously reported results suggest that the MgO dielectric is expected to have more defects and pinholes compared to Al_2O_3 characterized using scanning tunneling spectroscopy (STS) and structural analysis.[28−30] In order to prevent the formation of an IL between the metal/insulator (M/I) interface, a recent approach employs a Mg interlayer or graphene.[31−33] Despite this effort, the oxidation of the electrode is still a potential cause for IL formation, resulting in defective dielectric films.[33,34]

It is therefore imperative to address the issue with the IL formation in the development of high-quality ALD ultrathin dielectric films. In a recent work, we have developed a dynamic heating process to reduce the exposure of the metal surface (in high vacuum) before deposition of ALD-Al_2O_3 ultrathin films on Al and Fe using an *in vacuo* ultrahigh vacuum (UHV) sputtering sputtering/ALD process.[6] The M/I IL layer has been found to be effectively suppressed in both *in vacuo* STS studies of the 0.10−1.10 nm thickness ALD-Al_2O_3 layer and *ex situ* studies of the M/I/M devices.[1] It is particularly worth mentioning that an ε_r within 3% of the Al_2O_3 single-crystal bulk value has been demonstrated in 3.30−4.40 nm thick ALD-Al_2O_3 films by reducing the Al/ALD-Al_2O_3IL effect to a negligible level.[1,3,4] Unfortunately, direct growth of ultrathin ALD-MgO films on Al or Fe using similar *in vacuo* sputtering/ALD processes failed to generate high-quality dielectric films, which is attributed to different nucleation mechanisms of ALD-MgO and ALD-Al_2O_3 on metals.[28,29,34] This problem represents a general problem in the growth of ALD-dielectric on metals with an incompatible M/I interface that prevents uniform nucleation of an atomically thin ALD-dielectric film.

It should be pointed out that the incubation process in ALD of dielectric films is primarily generating oxides on the surface of metals to assist in a more efficient ligand exchange between precursors on the sample surface. This means the first ALD cycles are used for incubation of native oxides on the metal surface for nucleation of ALD-MgO.[33−35] Unfortunately, the native oxides are typically defective as shown in a recent study by our group.[3,4] ALD dielectric films grown on native oxides can have much degraded electronic and dielectric properties.[1,17,18,33−36] This means that the defective ALD-MgO films will not be suitable as tunnel barriers for MTJ applications. In order to resolve this issue, this work explores a novel seed-layer approach by *in situ* growth of a subnanometer thick ALD-Al_2O_3 seed layer (SL). SL is a high-quality dielectric and hence will have a negligible negative impact on the ALD-MgO growing on top as compared to the native oxide IL. We show a 0.55 nm thick ALD-Al_2O_3 SL enables high-quality ALD-MgO ultrathin (<5 nm) film growth. Remarkably, an ε_r up to 8.82−9.38 was achieved in ultrathin ALD-MgO dielectric films of thicknesses ∼3.30−4.95 nm, which is in contrast to the leaky ALD-MgO counterpart with significantly lower ε_r of ∼3.55−4.60 without the SL. These results are supported with a higher barrier height ∼1.50 eV for MgO/SL and dense nucleation with 100% coverage. However, a barrier height reduced to 0.80 eV for ALD-MgO without SL and ALD coverage reduced to less than 80%. The molecular dynamics simulation suggests that the SL layer allows for more regularly distributed Al and OH ligands leading to growth of denser and high-quality ALD-MgO dielectric as compared to the case on Al films, which is by its nature not self-terminating and is anticipated to have a relatively rougher terrain for subsequent growth of dielectric films. Thus, the SL approach may be applied to engineering the M/I interface for growth of high-quality ALD-dielectric ultrathin films on metals that would be otherwise incompatible.

METHODS

Fabrication of the M/I/M trilayers was carried out using an *in vacuo* in-house integrated UHV-ALD system.[6] First, a bilayer bottom electrode with 20 nm thick Nb covered with 7 nm thick Al was deposited using dc magnetron sputtering on a Si/SiO_2 substrate through a shadow mask for definition of an array of three capacitors. The deposition rate for the Nb was 1.70 nm/s and that for the Al was 0.50 nm/s. After the bottom metal electrode deposition, the sample was *in situ* transferred to the ALD chamber for growth of the ALD-Al_2O_3 SL and an ultrathin ALD-MgO dielectric (referred to as ALD-MgO/SL). The thickness of the SL was varied from 0.22 nm (2 ALD cycles) to 0.55 nm (5 ALD cycles), and the latter was found to be optimal based on the measurement of tunnel barrier height and the dielectric constant of the ALD-MgO/SL in the M/I/M trilayers. Figure S1 discuss in detail about the dielectric properties of ALD-MgO with different SL thickness. For a comparison, samples without a SL were fabricated in the same growth conditions. The optimal parameters for ALD preheating and substrate temperature based on our previous work were employed to prevent formation of a defective M/I IL, and the details can be found in our previous papers.[1,4] The trimethylaluminum (TMA, Sigma-Aldrich) was used as the Al precursor, which was maintained at room temperature during the ALD-Al_2O_3 growth. The optimal substrate temperature for the ALD-Al_2O_3 films is in the range of 200−220 °C based on our prior work.[1,3,4] For the ALD-MgO film growth, both substrates and bis(cyclopentadienyl)magnesium ($MgCP_2$, Sigma-Aldrich) Mg precursor were heated. The former was tested in the range of 200−255 °C, and the latter was in the range of 50−100 °C. The optimal substrate temperature has been found to be ∼200 °C for ALD-MgO growth, while the optimal $MgCp_2$ precursor temperature was found to be at 100 °C, which agrees well with prior reports.[35,36] In the following, all samples were fabricated using the optimal fabrication condition unless otherwise indicated. H_2O (Ultima grade, Fischer Scientific) was used as the oxygen precursor. The growth of the ALD-dielectric films occurs with alternating precursor pulses via a ligand exchange at the heated sample surface.[3] To ensure the formation of monolayer Al_2O_3 (or MgO) on the sample surface, a purge of the ALD system with N_2 gas (5 SCCM) between consecutive ALD precursor pulses was employed.[13] The thickness of ALD-Al_2O_3 (or ALD-MgO) per cycle is well calibrated to be ∼1.10−1.20 Å.[5,6,27,34,36] The thickness of the SL is hence approximately 0.55−0.60 nm, while that of the ALD-MgO films is in the range of 2.20−4.40 nm (or 20−40 ALD cycles). Fourier transform infrared spectroscopy (FTIR) was used to characterize the ALD-MgO films grown on the SiO_2 substrate. To obtain M/I/M capacitors, the top Al electrode ∼100 nm in thickness was sputtered after the ALD-MgO growth. Capacitance−voltage ($C-V$) and the leakage current vs voltage ($I-V$) measure-

DOI: 10.1021/acsami.9b05601
ACS Appl. Mater. Interfaces XXXX, XXX, XXX−XXX

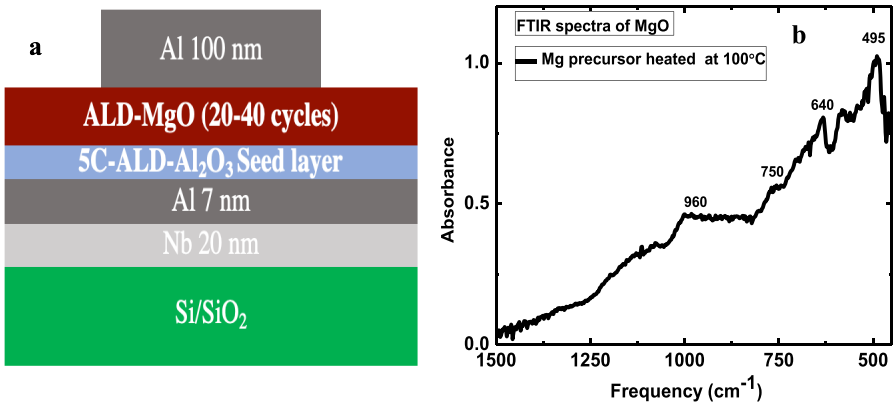

Figure 1. (a) Schematic of MIM trilayers fabricated with a SL for engineering the M/I interface and (b) FTIR absorbance spectrum taken on an ALD-MgO (20 C) film on the Si/SiO_2 substrate deposited at optimal conditions with a substrate temperature of 200 °C and source heated to 100 °C. The peaks are indexed to ALD-MgO.

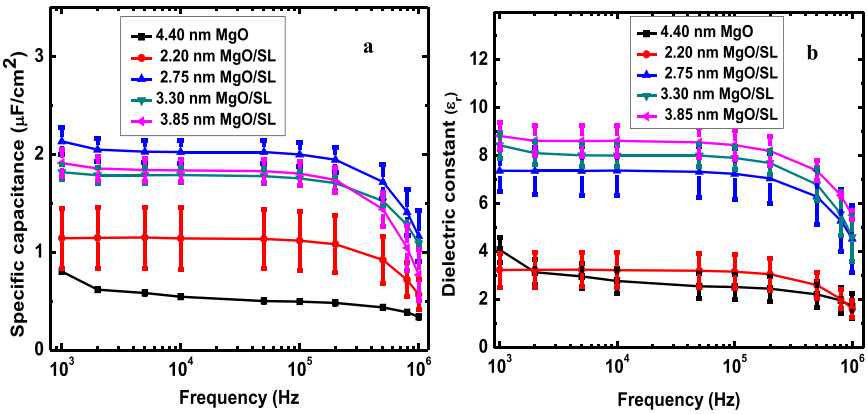

Figure 2. Variation of (a) specific capacitance and (b) dielectric constant with frequency for Al/MgO(2.20−3.85 nm)/SL(0.55 nm)/Al and Al/MgO(4.40) nm/Al MIM capacitor and three different junction areas, 400 × 100, 300 × 100, and 200 × 100 μm^2, fabricated using the previous method of a shadow mask.[1]

ments were carried out on the M/I/M devices using tungsten probes (25 μm in diameter, Lakeshore) in a probe station and an Agilent semiconductor analyzer.[1] *In vacuo* scanning tunneling spectroscopy (STS) spectra were taken on three half-cell (M/I) samples with the "I" layer of a total of 10 ALD cycles (10 C) of Al_2O_3 (10 C), Al_2O_3(5 C) + MgO (5 C), and MgO (10 C) to extract the effect of the SL on the dielectric properties and uniformity of the "I" layer.[1,3,4,37] A mechanically cleaved Pt−Ir tip was used for all STS studies at room temperature. IV and dI/dV spectra were taken simultaneously using a lock-in amplifier with a voltage modulation of 30 mV at 5 kHz, with a set point bias of 2.00 V and current of 200 pA to ensure the tip would not crash. The CBM, denoted as barrier height E_b, was estimated by the intersection of two bisquare-method linear fits to $\ln(dI/dV)$, similar to the method previously reported.[38] One line fits the band gap regime and the other the conduction band. These two regions are roughly linear in log scale. This $\ln(dI/dV)$ linear fit method was chosen over $I-V$ or $(dI/dV)/(I/V)$ fit methods for its insensitivity to high noise in the STS spectra.[39−41] Spectra were recorded in constant height mode, and the bias was sequentially ramped up and down 20 times, but no spectra averaging was used due to hysteresis from high local fields causing dielectric breakdown occasionally in later spectra of the set of 20. In order to shed light on the role of the SL, reactive molecular dynamics simulations were carried out using the ReaxFF interatomic potentials developed by Van Duin's group[42] as implemented in the LAMMPS MD code.[43,44] The use of ReaxFF interatomic potentials as the reactive force field approach[45,46] is necessary, as it gives an accurate depiction of the bond order and bond distance relationship and the dependency of the 3- and 4-body interactions toward the bond-order. This gives the capability to assess the bond breaking and bond forming mechanisms on the sample surface at the level of accuracy comparable to that from the density function theory (DFT) calculations[45] and is critical for the surface analysis.

RESULTS AND DISCUSSION

Figure 1a illustrates schematically the fabricated M/I/M trilayers. Figure 1b exhibits the FTIR spectrum taken on ALD-MgO (20 C) films deposited at optimal conditions with a substrate temperature of 200 °C and source heated to 100 °C. The appearance of absorption peaks at 495, 640, 750, and 960 cm^{-1} are indexed to MgO.[36,47] The intensity of peaks is low in our case as compared to previously reported results, which is most probably due to the fact that ZrO_2 nanoparticles in a photoetched tungsten screen were used for an enhancement of MgO peaks in prior studies.[36]

Figure 2a shows variation of specific capacitance (C_0) with frequency in the range from 1 kHz to 1 MHz measured on M/I/M capacitors with different "I" layers of ALD-MgO of thickness of 2.20, 2.75, 3.30, and 3.85 nm on the SL (colored curves). In addition, a device with 4.4 nm thick ALD-MgO without a SL is also included for comparison (black). The specific capacitance C_0 is defined from $C_0 = C/A = \varepsilon_0\varepsilon_r/t$ for different M/I/M devices and the dielectric thickness (t) in regards to the total thickness of the SL and the ALD-MgO thickness. The error bars were calculated using the three devices fabricated on the same sample with different capacitor

DOI: 10.1021/acsami.9b05601
ACS Appl. Mater. Interfaces XXXX, XXX, XXX−XXX

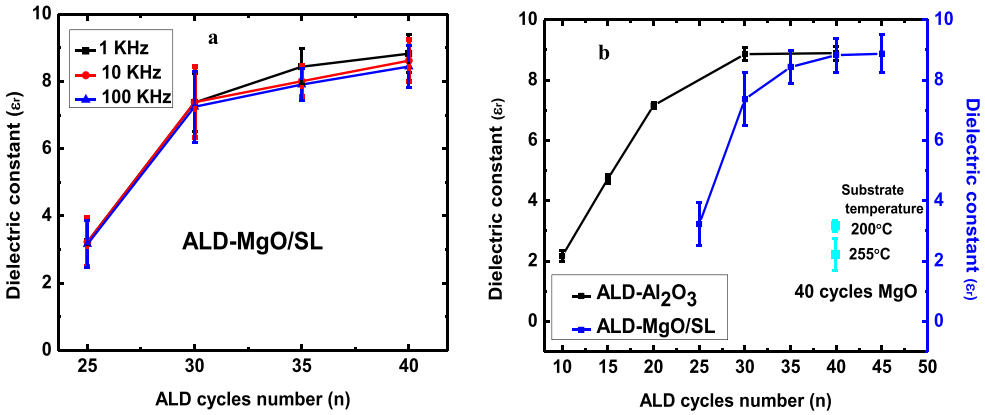

Figure 3. Variation of (a) dielectric constant for ALD-MgO/SL with ALD cycle numbers at different frequencies (1, 10, and 100 kHz) and (b) comparison of ALD-Al_2O_3 previously reported ALD-Al_2O_3 dielectric[1] (black) with ALD-MgO with SL (ALD-MgO/SL) (blue) and ALD-MgO without SL (ALD-MgO/Wo-SL) (cyan) deposited at substrate temperatures 200 and 255 °C

areas of 400 × 100, 300 × 100, and 200 × 100 μm^2, respectively. The M/I/M devices with the ALD-MgO/SL show an almost constant C_0 in the frequency range from 1 to 100 kHz (within 4−6% variation). With a further increase in the frequency, C_0 decreases due to dielectric loss.[48,49] Additionally, an almost constant C_0 was observed on the composite devices with the ALD-MgO/SL in the thickness range of 3.30−4.95 nm. At a smaller ALD-MgO/SL thickness of 2.75 nm, C_0 decreases considerably by 35−50% possibly due to the effect of electron tunneling, which will be discussed later. In contrast, the M/I/M ALD-MgO/WoSL devices show an overall lowering of C_0 by a factor >2 and more significant frequency dependence possibly due to defects initiated at the defective M/I interface.[50] Figure 2b shows variation of ε_r with frequency calculated using $\varepsilon_r = C_0 t/\varepsilon_0$ from the data in Figure 2a. The ε_r shows a similar frequency dependence to that of C_0, which is almost constant in the frequency range of 1−100 kHz with a small decrease of 4−5%. With further increasing frequencies, ε_r shows a larger decrease and this decrease is significantly larger on samples with lower ALD cycles. This larger variation of both C_0 and ε_r at higher frequencies can be explained by capacitive response and dielectric loss of the MIM capacitor with fast charging and discharging, since at large frequency all charges or dipoles cannot respond with fast polarity switching.[48,49] Our results indicate that these ALD-MgO capacitors are well suited for application in the frequency range up to 100 kHz but are less suitable for applications which requires higher frequency application. It should be noted that the independent measurement of the dielectric constant for the 0.55 nm seed layer of ALD-Al_2O_3 cannot be accomplished using the M/I/M structure since electron tunneling becomes possible as the thickness of the ALD-Al_2O_3 is comparable or below 2 nm and increases exponentially with decreasing ALD-Al_2O_3 thickness reported earlier.[1] Considering the comparable single-crystal bulk dielectric constants of Al_2O_3 (∼9.2) and MgO (∼9.8), negligible electron tunneling would occur at the dielectric thickness exceeding 2 nm and the dielectric constant of the composite ALD-MgO/SL film was calculated using the total thickness of the ALD-MgO and the ALD-Al_2O_3 seed layer.

Figure 3a shows the variation of ε_r with the ALD cycle number for ALD-MgO/SL at 1, 10, and 100 kHz. In the frequency range of 1−100 kHz, the ε_r values are comparable with 4−6% variation and they increase monotonically with the cycle number (or thickness) of the ALD-MgO. At 30−45 °C (or thickness of 3.30−4.95 nm including the SL), ε_r values of ∼8.82−9.38 have been obtained on the ALD-MgO/SL. To the best of our knowledge, this is the first time such a high ε_r approaching the single-crystal MgO's value is obtained in ultrathin ALD-MgO films. The effective oxide thickness or EOT = $t_{HiK} \cdot 3.90/\varepsilon_{Hik}$ used for evaluating high-K dielectric materials, where t_{HiK} and ε_{Hik} are the thickness and ε_r of the high-K dielectric materials, for the ALD-MgO/SL is estimated to be ∼1.45−2.05 nm. This suggest that the EOT of the ultrathin ALD-MgO/SL films are around 1.1−0.95 nm that is comparable to that for high-K HfO_2 of 3−4.5 nm in thickness and ε_{Hik} in the range of 10−18.5.[8,14,51]

Figure 3b shows a direct comparison of the ε_r values of the ALD-Al_2O_3, ALD-MgO/SL, and ALD-MgO/WoSL ultrathin films, illustrating a similar monotonic increasing trend with increasing ALD cycle numbers. At the optimal fabrication conditions reducing IL to a negligible thickness, ε_r remains constant around 8.90−9.00 for 3.30−4.40 nm thick ALD-Al_2O_3 films, which is comparable to the value for the Al_2O_3 single crystal[18] and is more than double of the best (ε_r ∼ 4.0) previously reported on 3.00 nm thick Al_2O_3 films.[17] The reduced ε_r values at smaller thicknesses are ascribed to the electron tunneling through the ALD-Al_2O_3 as reported in our previous work.[1] The similar thickness dependent trend on ALD-MgO/SL with ε_r values ∼8.82−9.38 for 3.30−4.95 nm and reduced ε_r values at smaller thicknesses have been observed. In addition, the ε_r values measured on two ALD-MgO/WoSL samples of 4.40 nm (cyan) are also included for comparison. However, 4.40 nm ALD-MgO/WoSL show a significantly lower ε_r of ∼3.55−4.60, which is indicative of the formation of a defective dielectric IL between the M/I interface with a possibility of nonuniform nucleation, which agrees with our detailed discussion later with STS. This argument agrees with previously reported results that MgO dielectric is expected to have more defects and pinholes compared to Al_2O_3,[28,29] suggesting the possibility of a different growth mechanism for MgO. A similar trend is shown in the ε_r of the ALD-MgO/SL samples (blue) indicating that the defect concentration has been significantly reduced with the adoption of the SL.

It should be mentioned that the ALD-MgO and ALD-Al_2O_3 films deposited at low temperatures of ∼200−220 °C are amorphous,[13] which means that no transmission electron

DOI: 10.1021/acsami.9b05601
ACS Appl. Mater. Interfaces XXXX, XXX, XXX−XXX

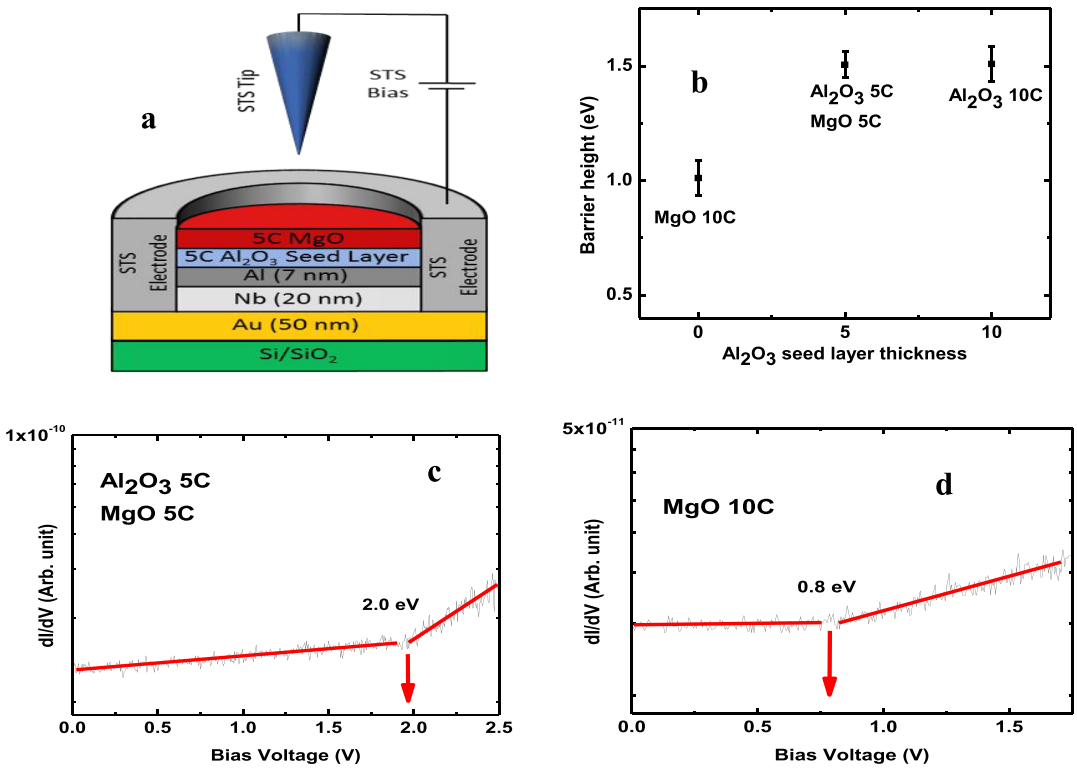

Figure 4. (a) Diagram of *in situ* deposited seed layer and tunnel barrier for STS analysis, (b) comparison of barrier heights for tunnel barriers of a total thickness of 10 C using different amounts of Al_2O_3 in their compositions, (c) representative dI/dV spectrum taken on a 5 C Al_2O_3/5 C MgO tunnel barrier, and (d) representative dI/dV spectrum taken on a 10 C MgO tunnel barrier.

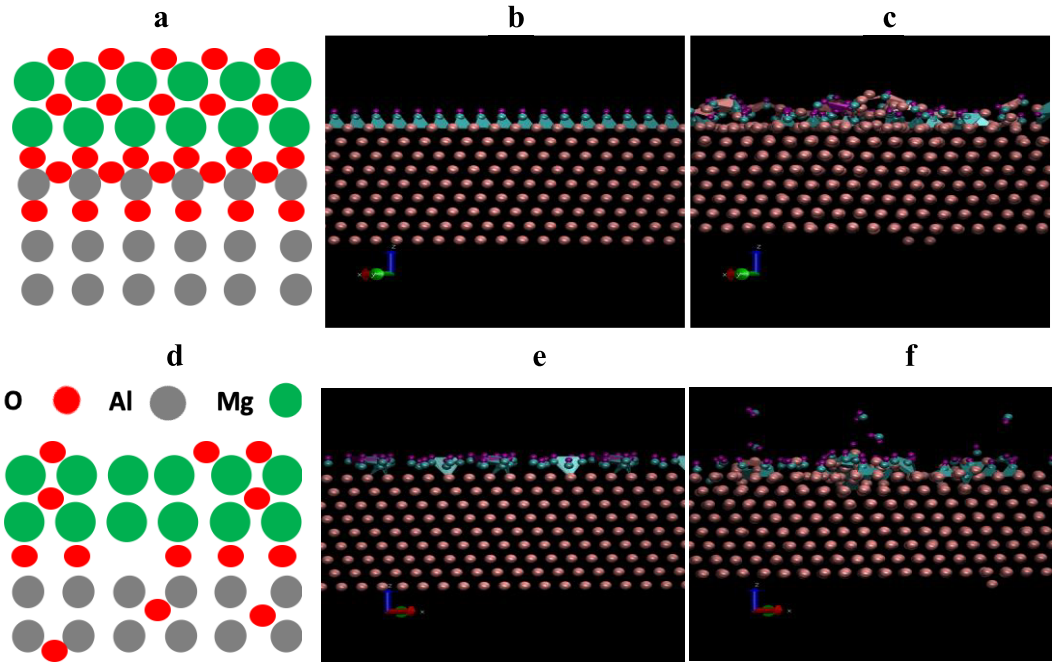

Figure 5. (a) Growth mechanism for ALD-MgO with the ALD-Al_2O_3 seed layer (dielectric with dense −OH nucleation); (b and c) side view of the atomic trajectories for the case of "orderly placed" (representing part a) −OH on the Al(111) surface after 0 and 25 000 fs, respectively; and (d) growth mechanism for ALD-MgO directly on Al(111) wetting layer (defective dielectric with poor −OH nucleation); (e and f) side view of the atomic trajectories for the case of "randomly-placed" (representing part d) −OH on the Al(111) wetting layer after 0 and 25 000 fs, respectively.

microscopy (TEM) diffraction can be obtained on them and on their interfaces with the metal electrode with an atomic resolution. To address this challenge, we recently implemented ultrahigh-vacuum scanning tunneling spectroscopy (STS) to study *in vacuo* the morphology and the electronic structure of the ultrathin ALD dielectric films with the thickness in the range of 0.1−1.0 nm. To complement the *in vacuo* STS measurement, devices of tunnel junctions and M/I/M trilayers

DOI: 10.1021/acsami.9b05601
ACS Appl. Mater. Interfaces XXXX, XXX, XXX−XXX

(like the ones reported in this work) have also been fabricated to characterize the ALD dielectric films using electric transport measurement. The agreement between the *in vacuo* STS and transport measurements on these devices can be found in our previous work.[1]

In an attempt to further understand the role of Al_2O_3 SL, Figure 4a shows a schematic of *in vacuo* STS analysis carried out on tunnel barriers with a combination of 10 ALD cycles (10 C) of Al_2O_3 (10 C), Al_2O_3(5 C) + MgO (5 C), and MgO (10 C). The 5C Al_2O_3/5C MgO and 10 C Al_2O_3 were found to have nearly identical barrier heights of ∼1.50 eV as in Figure 4b representing tunnel barriers with excellent quality on both samples. This is in drastic contrast to the 10 C MgO grown directly on the Al wetting layer resulting in a poor barrier height of ∼0.80 eV. These results illustrate the importance of SL to obtain a high-quality MgO dielectric. This difference may be observed by viewing Figure 4c,d, which illustrate the difference in the dI/dV spectra between the higher quality Al_2O_3/MgO and lower quality MgO barriers. The lower barrier height is due to defects present in the tunnel barrier, and these defects became more obvious while probing the surface since approximately 20% of the spectra were conductive or defective and the rest showed relatively low barrier heights. Furthermore, at other locations on the surface, there was too much noise for the scanning tip to even settle in order to take dI/dV spectra. Meaning that during ALD MgO growth without a SL, a complete layer of MgO is not grown and what is grown is of lower quality due to defects.

The transport and STS studies illustrate that the SL has a critical impact on the quality of the ultrathin ALD-MgO. In order to shed light on the effect of the SL, reactive MD simulations were carried out to compare the ALD-MgO growth on two surfaces with different configurations of OH groups distribution: OH groups distributed in a regular pattern on top of the Al(111) surface, which represents the case of MgO/SL as shown schematically in Figure 5a−c; and OH groups distributed disorderly on an Al(111) wetting layer, which represents the case of MgO/WoSL as shown in Figure 5d−f. The simulation results suggest that the OH pattern and density on the sample surface have a direct impact on the number of Mg−O bonds in the subsequent Mg precursor pulse. Figure 5b,c corresponds to the side view of atomic trajectories for "orderly placed" OH deposition after 0 and 25 000 fs, respectively. In this case, we barely see any occurrence of water vapor release implying the retention of OH molecules through the OH−OH lateral bonding formation of oxide clusters on the surface, presumably creating a denser dielectric film. Figure 5d shows a schematic of the proposed growth of MgO directly on an Al (111) surface, resulting in OH not self-terminating and consequently a defective IL in series with MgO dielectric. To support our argument, Figure 5e,f depicts the side view trajectories with "randomly-placed" OH groups on the Al(111) surface after 0 and 25 000 fs, respectively. Instead of forming a continuous OH layer as a result of the reaction between the adsorbed water molecules, some are deprotonated, releasing hydrogen and leaving oxygen on the Al surface. This leads to a low surface density and coverage of adsorbed OH on the Al surface and hence defective ALD-MgO in subsequent ALD growth. Therefore, the SL allows for dense and ordered OH ligands to assist ALD-MgO dielectric growth (see more simulation details in the Supporting Information).

The proposed ALD-MgO nucleation mechanism enabled by the SL is supported by comparison of leakage current density (J) measured on M/I/M capacitors with an "I" layer of 4.40 nm thick ALD-Al_2O_3, ALD-MgO/SL, and ALD-MgO/WoSL, respectively (Figure 6). This result indicates that the $J \sim 10^{-7}$ A/cm^2 for the 4.40 nm ALD-Al_2O_3 sample is the lowest among the three samples. The higher J values in the two ALD-MgO samples may be ascribed to the higher defect concentrations in these samples as compared to that of ALD-Al_2O_3. However, the implementation of a SL can effectively reduce the leakage by more than 1 order of magnitude compared to the ALD-MgO/WoSL. The detailed direct comparison of the I−V curves between ALD-Al_2O_3 and ALD-MgO/SL for the M/I/M capacitors is shown in the Supporting Information. However, direct ALD growth of MgO ultrathin films on Al and Fe has been found difficult. The ALD-MgO growth on metals shows that a large incubation period is necessary for complete hydroxylation that promotes the formation of native oxides on the metal surface.[33−35] We have attempted *in situ* ALD-MgO growth on Al and Fe but found the M/I/M structures are leaky even when the MgO film thickness is 4.4 nm. This is in contrast to high-quality ALD-Al_2O_3 ultrathin films of thickness as small as 0.1 nm on Al and Fe.[3,4] In order to resolve this issue in ALD growth of MgO on metals, this work develops a seed-layer approach to bypass the difficulty of ALD-MgO directly on metals. It should be pointed out that the ALD-Al_2O_3 seed layer differs fundamentally from native oxides on metal surfaces. As we have shown in our previous work with a direct comparison between ALD-Al_2O_3 and native AlO_x on an Al surface,[3] the former has a significantly reduced defect concentration.

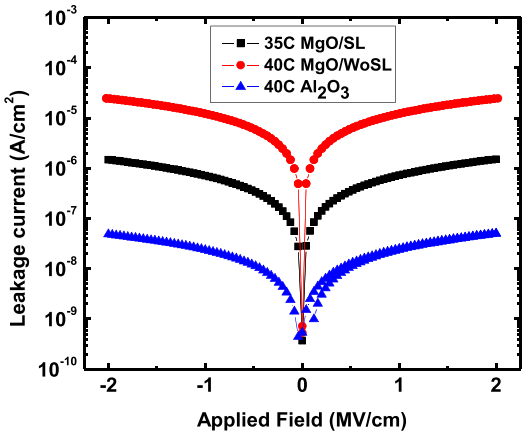

Figure 6. Comparison of leakage current for a total 4.40 nm ultrathin ALD dielectric films with ALD-Al_2O_3, ALD-MgO/SL, and ALD-MgO/WoSL for MIM capacitors using a log plot.

CONCLUSIONS

In summary, an ALD-Al_2O_3 SL of 0.55 nm thickness has been employed to grow M/I/M devices with ultrathin ALD-MgO dielectric films with thicknesses of 2.20−4.40 nm. The goal is to address critical issues in the nucleation of ALD-MgO directly on incompatible metals to form a sharp M/I interface. Our results indicate that the SL can convert such an incompatible metal surface to compatible by regulating the surface OH density/pattern and hence facilitating high-quality ALD-MgO growth. The ALD-MgO/SL films at 3.30−4.95 nm

DOI: 10.1021/acsami.9b05601
ACS Appl. Mater. Interfaces XXXX, XXX, XXX−XXX

thickness exhibit $\varepsilon_r \sim 8.82-9.40$, approaching the $\varepsilon_r \sim 9.80$ of the single-crystal MgO. STS demonstrates the ALD-MgO/SL with a barrier height of 1.50 eV with almost 100% coverage. In addition, our MD simulations indicate that the ALD-MgO/SL layer allows regularly distributed Al and OH ligands leading to growth of denser and high-quality MgO dielectric. In contrast, the ALD-MgO/WoSL of comparable thickness is defective with a low ε_r of 3.55−4.66 along with nonuniform nucleation on the Al surface with a significant portion of the Al surface remaining conductive as confirmed using the *in vacuo* STS. The reactive MD simulations on MgO growth directly on Al provide insights showing a nonself-terminating surface with rougher terrain for subsequent growth of a defective dielectric film. These results illustrate that the SL approach is promising to engineer otherwise incompatible M/I interfaces to enable *in vacuo* growth of M/I/M trilayers of an ultrathin leak-free dielectric with a low defect concentration required in a large variety of microelectronic and memory applications.

■ ASSOCIATED CONTENT

Supporting Information

The Supporting Information is available free of charge on the ACS Publications website at DOI: 10.1021/acsami.9b05601.

Effect of Al_2O_3 seed-layer on the dielectric and electrical properties of ultrathin MgO fabricated using *in situ* atomic layer deposition (PDF)

Video of the reactive molecular dynamics simulations showing the side view of the atomic trajectories for ALD-MgO/SL (MP4)

Video of the reactive molecular dynamics simulations showing the side view of the atomic trajectories for ALD-MgO/WoSL (MP4)

■ AUTHOR INFORMATION

Corresponding Authors

*E-mail: jagaran@ku.edu.

*E-mail: jwu@ku.edu/

ORCID

Jagaran Acharya: 0000-0003-1129-0974

Author Contributions

J.A. and J.W. designed the experiment. J.A. prepared the samples for MIM and performed the dielectric properties characterization and most of the analysis. R.G. helped with STS sample fabrication and measurement. D.R. and R.S. contributed to the molecular dynamics simulations. All authors contributed for the discussion of results. J.A. and J.W. led the effort in the development of the manuscript.

Notes

The authors declare no competing financial interest.

■ ACKNOWLEDGMENTS

This research was supported in part by NSF Contract Nos. NSF-DMR-1508494 and NSF-ECCS-1809293/1809284 and ARO Contract No. W911NF-16-1-0029.

■ REFERENCES

(1) Acharya, J.; Wilt, J.; Liu, B.; Wu, J. Probing the Dielectric Properties of Ultrathin Al/Al2o3/Al Trilayers Fabricated Using in Situ Sputtering and Atomic Layer Deposition. *ACS Appl. Mater. Interfaces* **2018**, *10*, 3112−3120.

(2) Yuasa, S.; Nagahama, T.; Fukushima, A.; Suzuki, Y.; Ando, K. Giant Room-Temperature Magnetoresistance in Single-Crystal Fe/Mgo/Fe Magnetic Tunnel Junctions. *Nat. Mater.* **2004**, *3*, 868−871.

(3) Wilt, J.; Sakidja, R.; Goul, R.; Wu, J. Z. Effect of an Interfacial Layer on Electron Tunneling through Atomically Thin Al2o3 Tunnel Barriers. *ACS Appl. Mater. Interfaces* **2017**, *9*, 37468−37475.

(4) Wilt, J.; Gong, Y.; Gong, M.; Su, F.; Xu, H.; Sakidja, R.; Elliot, A.; Lu, R.; Zhao, S.; Han, S.; Wu, J. Z. Atomically Thin Al 2 O 3 Films for Tunnel Junctions. *Phys. Rev. Appl.* **2017**, *7*, 064022.

(5) Elliot, A. J.; Malek, G.; Wille, L.; Lu, R.; Han, S.; Wu, J. Z.; Talvacchio, J.; Lewis, R. M. Probing the Nucleation of in Atomic Layer Deposition on Aluminum for Ultrathin Tunneling Barriers in Josephson Junctions. *IEEE Trans. Appl. Supercond.* **2013**, *23*, 1101405−1101405.

(6) Elliot, A. J.; Malek, G. A.; Lu, R.; Han, S.; Yu, H.; Zhao, S.; Wu, J. Z. Integrating Atomic Layer Deposition and Ultra-High Vacuum Physical Vapor Deposition for in Situ Fabrication of Tunnel Junctions. *Rev. Sci. Instrum.* **2014**, *85*, 073904.

(7) Robertson, J.; Wallace, R. M. High-K Materials and Metal Gates for Cmos Applications. *Mater. Sci. Eng., R* **2015**, *88*, 1−41.

(8) Kim, S.; Woo, S.; Kim, H.; Kim, I.; Lee, K.; Jeong, W.; Park, T.; Jeon, H. Atomic Layer Deposition of Hfo2 Thin Films on Ultrathin Sio2 Formed by Remote Plasma Oxidation. *J. Korean Phys. Soc.* **2008**, *52*, 1103.

(9) Wilk, G. D.; Wallace, R. M.; Anthony, J. High-K Gate Dielectrics: Current Status and Materials Properties Considerations. *J. Appl. Phys.* **2001**, *89*, 5243−5275.

(10) Dietrich, C.; Boyen, H.-G.; Koslowski, B. Characterization of Ultrathin Insulating Al2o3 Films Grown on Nb (110)/Sapphire (0001) by Tunneling Spectroscopy and Microscopy. *J. Appl. Phys.* **2003**, *94*, 1478−1484.

(11) Lu, R.; Elliot, A. J.; Wille, L.; Mao, B.; Han, S.; Wu, J. Z.; Talvacchio, J.; Schulze, H. M.; Lewis, R. M.; Ewing, D. J.; Yu, H. F.; Xue, G. M.; Zhao, S. P. Fabrication of Josephson Junctions Using in Situ Magnetron Sputtering and Atomic Layer Deposition. *IEEE Trans. Appl. Supercond.* **2013**, *23*, 1100705−1100705.

(12) Elliott, S. D. Atomic-Scale Simulation of Ald Chemistry. *Semicond. Sci. Technol.* **2012**, *27*, 074008.

(13) George, S. M. Atomic Layer Deposition: An Overview. *Chem. Rev.* **2010**, *110*, 111−131.

(14) Lee, K.; Lee, Y.; Chang, P.; Huang, M.; Chang, Y.; Hong, M.; Kwo, J. Achieving 1 Nm Capacitive Effective Thickness in Atomic Layer Deposited Hf O 2 on in 0.53 Ga 0.47 As. *Appl. Phys. Lett.* **2008**, *92*, 252908.

(15) Kim, H.; McIntyre, P. C. Atomic Layer Deposition of Ultrathin Metal-Oxide Films for Nano-Scale Device Applications. *J. Korean Phys. Soc.* **2006**, *48*, 5−17.

(16) Martin, D.; Grube, M.; Weinreich, W.; Müller, J.; Weber, W. M.; Schröder, U.; Riechert, H.; Mikolajick, T. Mesoscopic Analysis of Leakage Current Suppression in Zro2/Al2o3/Zro2 Nano-Laminates. *J. Appl. Phys.* **2013**, *113*, 194103.

(17) Groner, M.; Elam, J.; Fabreguette, F.; George, S. M. Electrical Characterization of Thin Al 2 O 3 Films Grown by Atomic Layer Deposition on Silicon and Various Metal Substrates. *Thin Solid Films* **2002**, *413*, 186−197.

(18) Birey, H. Thickness Dependence of the Dielectric Constant and Resistance of Al2o3 Films. *J. Appl. Phys.* **1977**, *48*, 5209−5212.

(19) Krupka, J.; Geyer, R. G.; Kuhn, M.; Hinken, J. H. Dielectric Properties of Single Crystals of Al2o3, Laalo3, Ndgao3, Srtio3, and Mgo at Cryogenic Temperatures. *IEEE Trans. Microwave Theory Tech.* **1994**, *42*, 1886−1890.

(20) Raj, A. M. E.; Jayachandran, M.; Sanjeeviraja, C. Fabrication Techniques and Material Properties of Dielectric Mgo Thin Films—a Status Review. *CIRP Journal of Manufacturing Science and Technology* **2010**, *2*, 92−113.

(21) Mantovan, R.; Vangelista, S.; Kutrzeba-Kotowska, B.; Lamperti, A.; Manca, N.; Pellegrino, L.; Fanciulli, M. Fe 3-Δo4 /Mgo/Co Magnetic Tunnel Junctions Synthesized by Full in Situ Atomic Layer

DOI: 10.1021/acsami.9b05601
ACS Appl. Mater. Interfaces XXXX, XXX, XXX−XXX

and Chemical Vapour Deposition. *J. Phys. D: Appl. Phys.* **2014**, *47*, 102002.

(22) Mantovan, R.; Vangelista, S.; Kutrzeba-Kotowska, B.; Cocco, S.; Lamperti, A.; Tallarida, G.; Mameli, D.; Fanciulli, M. Synthesis of Magnetic Tunnel Junctions with Full in Situ Atomic Layer and Chemical Vapor Deposition Processes. *Thin Solid Films* **2012**, *520*, 4820−4822.

(23) Yoon, J. G.; Kim, K. Growth of (111) Oriented Mgo Film on Si Substrate by the Sol-Gel Method. *Appl. Phys. Lett.* **1995**, *66*, 2661−2663.

(24) Wang, D.; Nordman, C.; Daughton, J. M.; Qian, Z.; Fink, J. 70% Tmr at Room Temperature for Sdt Sandwich Junctions with Cofeb as Free and Reference Layers. *IEEE Trans. Magn.* **2004**, *40*, 2269−2271.

(25) Boo, J.-H.; Yu, K.-S.; Koh, W.; Kim, Y. Preparation of Mgo Films on Gaas by Metalorganic Chemical Vapor Deposition. *Mater. Lett.* **1996**, *26*, 233−236.

(26) Fork, D.; Ponce, F.; Tramontana, J.; Geballe, T. Epitaxial Mgo on Si (001) for Y-Ba-Cu-O Thin-Film Growth by Pulsed Laser Deposition. *Appl. Phys. Lett.* **1991**, *58*, 2294−2296.

(27) Vangelista, S.; Mantovan, R.; Lamperti, A.; Tallarida, G.; Kutrzeba-Kotowska, B.; Spiga, S.; Fanciulli, M. Low-Temperature Atomic Layer Deposition of Mgo Thin Films on Si. *J. Phys. D: Appl. Phys.* **2013**, *46*, 485304.

(28) Kohn, A.; Kovács, A.; Uhrmann, T.; Dimopoulos, T.; Brückl, H. Structural and Electrical Characterization of Sio2/Mgo(001) Barriers on Si for a Magnetic Transistor. *Appl. Phys. Lett.* **2009**, *95*, 042506.

(29) Mather, P.; Read, J.; Buhrman, R. Disorder, Defects, and Band Gaps in Ultrathin (001) Mgo Tunnel Barrier Layers. *Phys. Rev. B: Condens. Matter Mater. Phys.* **2006**, *73*, 205412.

(30) Thomas, A.; Drewello, V.; Schäfers, M.; Weddemann, A.; Reiss, G.; Eilers, G.; Münzenberg, M.; Thiel, K.; Seibt, M. Direct Imaging of the Structural Change Generated by Dielectric Breakdown in Mgo Based Magnetic Tunnel Junctions. *Appl. Phys. Lett.* **2008**, *93*, 152508.

(31) Martin, M.-B.; Dlubak, B.; Weatherup, R. S.; Yang, H.; Deranlot, C.; Bouzehouane, K.; Petroff, F.; Anane, A.; Hofmann, S.; Robertson, J.; Fert, A.; Seneor, P. Sub-Nanometer Atomic Layer Deposition for Spintronics in Magnetic Tunnel Junctions Based on Graphene Spin-Filtering Membranes. *ACS Nano* **2014**, *8*, 7890−7895.

(32) Dlubak, B.; Martin, M.-B.; Weatherup, R. S.; Yang, H.; Deranlot, C.; Blume, R.; Schloegl, R.; Fert, A.; Anane, A.; Hofmann, S.; Seneor, P.; Robertson, J. Graphene-Passivated Nickel as an Oxidation-Resistant Electrode for Spintronics. *ACS Nano* **2012**, *6*, 10930−10934.

(33) Ryu, S. W.; Song, J.-G.; Kim, H. G.; Kim, H.; Lee, H.-B.-R. Interlayer-Assisted Atomic Layer Deposition of Mgo as a Magnetic Tunneling Junction Insulators. *J. Alloys Compd.* **2018**, *747*, 505−510.

(34) Song, J.-G.; Park, J.; Yoon, J.; Kim, K.; Jang, Y.; Kim, K.; Kim, H. Investigation of Atomic Layer Deposition of Magnesium Oxide on a Cofeb Layer for Three-Dimensional Magnetic Tunneling Junctions. *J. Alloys Compd.* **2014**, *588*, 716−719.

(35) Wang, H.; Fu, K. Nucleation and Growth of Mgo Atomic Layer Deposition: A Real-Time Spectroscopic Ellipsometry Study. *J. Vac. Sci. Technol., A* **2013**, *31*, 06F101.

(36) Burton, B.; Goldstein, D.; George, S. Atomic Layer Deposition of Mgo Using Bis (Ethylcyclopentadienyl) Magnesium and H2o. *J. Phys. Chem. C* **2009**, *113*, 1939−1946.

(37) Wilt, J.; Goul, R.; Acharya, J.; Sakidja, R.; Wu, J. Z. In Situ Atomic Layer Deposition and Electron Tunneling Characterization of Monolayer Al2o3 on Fe for Magnetic Tunnel Junctions. *AIP Adv.* **2018**, *8*, 125218.

(38) Ugeda, M. M.; Bradley, A. J.; Shi, S.-F.; da Jornada, F. H.; Zhang, Y.; Qiu, D. Y.; Ruan, W.; Mo, S.-K.; Hussain, Z.; Shen, Z.-X.; Wang, F.; Louie, S. G.; Crommie, M. F. Giant Bandgap Renormalization and Excitonic Effects in a Monolayer Transition Metal Dichalcogenide Semiconductor. *Nat. Mater.* **2014**, *13*, 1091−1095.

(39) Feenstra, R. M.; Gaan, S.; Meyer, G.; Rieder, K. Low-Temperature Tunneling Spectroscopy of Ge (111) C (2× 8) Surfaces. *Phys. Rev. B: Condens. Matter Mater. Phys.* **2005**, *71*, 125316.

(40) Dorneles, L.; Schaefer, D.; Carara, M.; Schelp, L. The Use of Simmons' Equation to Quantify the Insulating Barrier Parameters in Al/Alo X/Al Tunnel Junctions. *Appl. Phys. Lett.* **2003**, *82*, 2832−2834.

(41) Ugeda, M. M.; Bradley, A. J.; Shi, S.-F.; da Jornada, F. H.; Zhang, Y.; Qiu, D. Y.; Ruan, W.; Mo, S.-K.; Hussain, Z.; Shen, Z.-X.; Wang, F.; Louie, S. G.; Crommie, M. F. Giant Bandgap Renormalization and Excitonic Effects in a Monolayer Transition Metal Dichalcogenide Semiconductor. *Nat. Mater.* **2014**, *13*, 1091.

(42) Hong, S.; van Duin, A. C. T. Atomistic-Scale Analysis of Carbon Coating and Its Effect on the Oxidation of Aluminum Nanoparticles by Reaxff-Molecular Dynamics Simulations. *J. Phys. Chem. C* **2016**, *120*, 9464−9474.

(43) http://lammps.sandia.gov (accessed January 19, 2019).

(44) Plimpton, S. Fast Parallel Algorithms for Short-Range Molecular Dynamics. *J. Comput. Phys.* **1995**, *117*, 1−19.

(45) Senftle, T.; Hong, S.; Islam, M.; Kylasa, S. B.; Zheng, Y.; Shin, Y. K.; Junkermeier, C.; Engel-Herbert, R.; Janik, M.; Aktulga, H. M.; Verstraelen, T.; Grama, A. Y.; van Duin, A. C. T. The Reaxff Reactive Force-Field: Development, Applications, and Future Directions. *npj Comput. Mater.* **2016**, *2*, 15011.

(46) van Duin, A. C. T.; Dasgupta, S.; Lorant, F.; Goddard, W. A. Reaxff: A Reactive Force Field for Hydrocarbons. *J. Phys. Chem. A* **2001**, *105*, 9396−9409.

(47) Gourley, J.; Runciman, W. Multiphonon Infrared Absorption Spectra of Mgo and Cao. *J. Phys. C: Solid State Phys.* **1973**, *6*, 583.

(48) Ki Min, B.; Kim, S. K.; Jun Kim, S.; Ho Kim, S.; Kang, M.-A.; Park, C.-Y.; Song, W.; Myung, S.; Lim, J.; An, K.-S. Electrical Double Layer Capacitance in a Graphene-Embedded Al2o3 Gate Dielectric. *Sci. Rep.* **2015**, *5*, 16001.

(49) Srivastava, A.; Mangla, O.; Gupta, V. Study of La-Incorporated Hfo2Mim Structure Fabricated Using Pld System for Analog/Mixed Signal Applications. *IEEE Trans. Nanotechnol.* **2015**, *14*, 612−618.

(50) Ortiz, C. R.; Pantojas, V. M.; Otaño-Rivera, W. Effect of Annealing on the Electrical Properties of Insulating Aluminum Nitride in Mim and Mis Structures. *Solid-State Electron.* **2014**, *91*, 106−111.

(51) Hu, H.; Zhu, C.; Lu, Y.; Li, M.; Cho, B. J.; Choi, W. A High Performance Mim Capacitor Using Hfo 2 Dielectrics. *IEEE Electron Device Lett.* **2002**, *23*, 514−516.

DOI: 10.1021/acsami.9b05601
ACS Appl. Mater. Interfaces XXXX, XXX, XXX−XXX